J Mater Sci: Mater Med (2010) 21:329–341
DOI 10.1007/s10856-009-3836-8

Adhesion, spreading and osteogenic differentiation of mesenchymal stem cells cultured on micropatterned amorphous diamond, titanium, tantalum and chromium coatings on silicon

Sami Myllymaa · Emilia Kaivosoja · Katja Myllymaa · Tarvo Sillat · Hannu Korhonen · Reijo Lappalainen · Yrjö T. Konttinen

Received: 22 May 2009 / Accepted: 22 July 2009 / Published online: 5 August 2009

Abstract It was hypothesized that human mesenchymal stromal cell (hMSC) can be guided by patterned and plain amorphous diamond (AD), titanium (Ti), tantalum (Ta) and chromium (Cr) coatings, produced on silicon wafer using physical vapour deposition and photolithography. At 7.5 h hMSCs density was 3.0–3.5× higher ($P < 0.0003$, except Ti) and cells were smaller (68 vs. 102 μm, P 0.000006–0.02) on patterns than on silicon background. HMSC-covered surface of the background silicon was lower on Ti than AD patterns ($P = 0.015$), but at 5 days this had reversed ($P = 0.006$). At 7.5 h focal vinculin adhesions and actin cytoskeleton were outgoing from pattern edges so cells assumed geometric square shapes. Patterns allowed induced osteogenesis, but less effectively than plain surfaces, except for AD, which could be used to avoid osseointegration. All these biomaterial patterns exert direct early, intermediate and late guidance on hMSCs and osteogenic differentiation, but indirect interactions exist with cells on silicon background.

S. Myllymaa and E. Kaivosoja contributed equally to this work.

S. Myllymaa · K. Myllymaa · H. Korhonen · R. Lappalainen (✉)
Department of Physics, University of Kuopio, Yliopistonranta 1 F, 70210 Kuopio, Finland
e-mail: reijo.lappalainen@uku.fi

S. Myllymaa
e-mail: sami.myllymaa@uku.fi

E. Kaivosoja · Y. T. Konttinen
Department of Medicine, Institute of Clinical Medicine, Helsinki University Central Hospital, Haartmaninkatu 8, 00029 Helsinki, Finland

K. Myllymaa
Microsensor Laboratory, School of Engineering and Technology, Savonia University of Applied Sciences, Microkatu 1C, 70201 Kuopio, Finland

T. Sillat
Department of Anatomy, Institute of Biomedicine, University of Helsinki, Haartmaninkatu 8, 00014 Helsinki, Finland

Y. T. Konttinen
ORTON Orthopaedic Hospital of the Invalid Foundation, Tenholantie 10, 00280 Helsinki, Finland

Y. T. Konttinen
COXA Hospital for Joint Replacement, Biokatu 6b, 33520 Tampere, Finland

1 Introduction

The effect of the surface texture produced by various etching and laser micromachining techniques has been mostly studied in the micrometer and sub-micrometer scale [1–3]. Surface texture has been employed in attempts to control cellular adhesion, proliferation, differentiation and contact guidance of cells [4, 5]. Recently much attention has been paid to human mesenchymal stromal cells (hMSC) due to their role in tissue repair and their potential in regenerative medicine and tissue engineering applications. They are able to undergo asymmetric cell divisions to maintain themselves and to provide progenitors to several differentiated mesenchymal cells [6]. In tissue engineering applications such cells are grown on biomaterial scaffold, which provides structural support and substrate for cellular adhesion. Therefore, knowledge on cell–biomaterial interactions has become increasingly important. In this study effects of metals (commonly used as such or as alloys in implants and scaffolds) on the hMSCs were studied and compared to in house produced amorphous diamond (AD), which has been developed for potential use as implant coating [7, 8].

Stiehler et al. has earlier reported results on the effect of tantalum (Ta), titanium (Ti), and chromium (Cr) coatings on cells using plain surfaces [9]. This was a solid base in the present work extended by producing 75 μm × 75 μm square patterns of these metals using physical vapour deposition combined with photolithography. In addition, these metals were compared to similarly patterned AD. Apart from tissue engineering applications, cell–biomaterial interactions assume importance due to the biomaterial–cell contacts, which develop upon implantation of any prosthesis, stent, shunt or other implant. It is envisioned that in the future the use of intelligent implants, like bio micro-electro-mechanical-systems (bio-MEMS implants), which are typically produced on silicon background, will increase. Therefore, silicon was used as the background material for the patterned and plain material surfaces analyzed in this study. From another point of view, hMSCs can be regarded as sensitive and versatile cellular sensors, which can be used to explore the biocompatibility of biomaterials. Cellular adhesion, spreading and differentiation act then as indicators of the quality of the cell–biomaterial interactions and provide information on eventual differences between different textured and plain materials. Previous studies of hMSCs on micropatterned surfaces have focused on polymers or functionalized patterns [10–17] and nanotopography of Ti on hMSCs [18]. This is the first study focusing on the morphology, adhesion, spreading and osteogenic differentiation of hMSC on well-characterized, micro-patterned metallic (Ti, Ta, Cr) and ceramic (AD) coatings on silicon background. It was hypothesized that micro-patterned materials differently guide hMSC behaviour.

2 Materials and methods

2.1 Sample fabrication

Silicon wafers (p-type, 2″, ⟨100⟩, Si-Mat, Landsberg am Lech, Germany) were used as substrate material. Ti, Ta and Cr depositions were carried out by magnetron sputtering technique and AD depositions by filtered pulsed plasma arc discharge method [7, 8]. Samples were photo-lithographically patterned via a lift-off process. The size of each sample was 10 mm × 10 mm in which the micropatterned area was 8 mm × 8 mm. Patterns consisted of 75 μm squares with 100 μm spacing between squares in two orthogonal directions. Thus, the pattern/background surface area ratio is about 0.18 in the patterned (8 mm × 8 mm) region. Patterns were designed by CleWin layout software (Wieweb Software, Hengelo, The Netherlands). Chrome-plated soda lime glass photomasks were supplied by Mikcell Ltd. (Ii, Finland). Samples without patterning were fabricated for osteogenic differentiation.

Silicon wafers were dry-baked and coated with 20% hexamethyldisilazane (Riedel-de Haen Laborchemikalien, Seelze, Germany) in xylene to remove moisture and to improve the adhesion between photoresist and silicon. A negative photoresist (ma-N 1420, Microresist Technology GmbH, Berlin, Germany) was spun at 5000 rpm for 30 s and pre-baked on a hot plate for 2 min at 100°C. The exposure was carried out by Karl Suss MA45 exposure tool (Suss Microtec Inc., Waterbury Center, VT, USA) through the photomask for 14 s at 365 nm. Unexposed ma-N 1420 was removed by developing 1.5 min in ma-D 533s developer (Microresist Technology GmbH). Samples were rinsed in deionized water to remove organic residues.

Magnetron sputtering (Stiletto Serie ST20, AJA International Inc., North Scituate, MA, USA) in argon plasma was used to deposit metal films from high purity (99.6% or better) target materials (Goodfellow Metals, Huntingdon, England). Acceleration voltage of 400–500 V and 3–4 × 10^{-4} mbar argon pressure were used for 5 min to deposit 200 nm thick films. In the filtered pulsed plasma arc discharge method to deposit AD coatings [19, 20] carbon plasma pulses were produced by discharging the capacitor bank between the graphite cathode and anode. Plasma pulses of 1–7 Hz frequency were steered and deflected with electric coils to the sample surface. An extremely thin adhesion layer was produced by high energy plasma accelerated using a capacitor ($C = 16$ μF) voltage of 6000 V followed by a low energy deposition run at 500 V to produce a 200 nm thick coating.

After deposition the wafers were ultrasonicated in mr-Rem 660 resist remover (Microresist Technology GmbH) at room temperature to remove the ma-N 1420 resist. Thin film deposited on the top of photoresist was washed away revealing the final micropatterns, which were cut to 10 mm × 10 mm pieces before sonication for a few minutes in 7× detergent (OneMed Ltd., Vantaa, Finland), ethanol and deionized water to remove photoresist residues and silicon dust from scribing and cutting.

2.2 Sample sterilization

Samples were immersed in Petri-dishes for 30 min in 70% ethanol, which was removed by pouring and evaporation before packaging in sterile bags and sterilization using 31.8 kGy gamma irradiation from a Co-60 source (Gammacell 220, Atomic Energy of Canada Limited, Mississauga, Canada).

2.3 Atomic force microscopy (AFM)

The nanometer scale surface topography was analyzed using a PSIA XE-100 (Park Systems Corp., Suwon, Korea) atomic force microscope at ambient temperature and humidity. Aluminum coated silicon cantilevers (Acta-10,

ST Instruments B.V., LE Groot-Ammers, The Netherlands) were used in a non-contact mode to scan the surface across an area of 2 × 2 μm with a scanning rate of 0.25 Hz. Average surface roughness (R_a) and peak-to-valley roughness (R_{pv}) were determined from 6 random AFM images using the instrument analysis software (XIA).

2.4 Contact angle and surface energy measurements

Samples were ultrasonicated in ethanol and deionized water and dried. Contact angles were measured using the sessile drop (15 μl) method with a custom made apparatus using an optical SZ-PT Olympus microscope equipped with a Olympus Camedia C-3030ZOOM digital camera (Olympus Corp., Tokyo, Japan). To access the total surface energy and its polar/dispersive component, contact angles for water (polar) and diiodomethane (non-polar) were measured within 5 s after placement of the drop at +22°C and 45% relative humidity. The spreading pressure was not taken into account. The drop image was stored and an image analysis software GIMP (www.gimp.org) was used to determine the left and right margin contact angles of five sessile drops for calculation of the average contact angle.

The dispersive γ_S^D and polar γ_S^P components were estimated using the geometrical equation [21]:

$$(1+\cos\,\theta)\gamma_{_L} = 2\left(\left(\gamma_S^D\gamma_L^D\right)^{1/2}+\left(\gamma_S^P\gamma_L^P\right)^{1/2}\right), \quad (1)$$

where (θ) is measured (averaged) contact angle value, superscript D labels the dispersive component and P the polar component of the surface tension and the subscripts S and L stand for solid and liquid, respectively. γ_L, γ_L^D and γ_L^P stand for total surface energy of liquid, its dispersive component and its polar component, respectively [22]. Total surface energy (γ_S) is the sum of its dispersive and polar components.

2.5 Cell cultures

Human hMSC (Poietics™, Lonza, Basel, Switzerland) were cultured on 10 cm Petri dishes (Corning Inc., New York, USA) using Lonza Mesenchymal Stem Cell Basal Medium with Mesenchymal Cell Growth Supplement (MSCGM) containing L-glutamine and penicillin (SEM experiment) or GA-1000 (Gentamicin/Amphotericin-B). The cells were cultured at +37°C in humid 5% CO_2-in-air. The cell monolayer was washed twice with phosphate buffered 140 mM saline (PBS, pH 7.4) and the cells were detached using 2.5 mg/ml trypsin in PBS-EDTA (0.05 ml/cm^2) at room temperature for 5 min. An equal volume of temperature equilibrated MSCGM was added. The suspension was transferred to a Falcon tube and trypsin was removed by centrifuging the cells at 600×g for 5 min. Cells were resuspended in culture medium and seeded onto the biomaterial surfaces at 0.52 × 10^4 cm^{-2} density. The cells were cultured for 7.5 h or 5 days (80% confluence).

For osteogenic induction the 7th passage cells were seeded at 0.31 × 10^4 cm^{-2}. Half of the samples were induced 24 h after seeding by replacing MSCGM with Osteogenesis Induction Medium (Lonza). Induced hMSCs were fed every 3–4 days with fresh Osteogenesis Induction Medium. Non-induced control hMSCs were fed with MSCGM using the same schedule. The development of the osteoblastic phenotype was followed using differentiation markers. TC-treated polystyrene 12-well microplates (Corning Inc.) were used in all experiments. The markers used were alkaline phosphatase activity as an early day 14 marker, osteocalcin as an intermediate day 17 marker and mineralization as late day 21 marker [23].

2.6 Scanning electron microscopy

At least three parallel hMSC samples were analyzed at 7.5 h and at 5 days. After incubation, samples were transferred to new tissue culture plates, washed twice with PBS and fixed in 2.5% glutaraldehyde (Sigma Chemical, St. Louis, MO, USA) for overnight at +4°C. Samples were washed 3 × 10 min with PBS, dehydrated in ethanol/water mixtures of 50, 70, 80, and 90% for 5 min each and in 96% and twice in 100% for 10 min. Dehydration was completed using Bal-Tec CPD 030 Critical point drying unit (BAL-TEC AG, Balzers, Liechtenstein). Samples were mounted on SEM stubs, coated with platinum with an Agar sputter device (AGAR, Stansted, England) and examined using a Zeiss DSM 962 scanning electron microscope (Carl Zeiss, Oberkochen, Germany) at an accelerating voltage of 8 kV with four images being taken from each sample.

At 7.5 h cells on patterns or on background were marked with a different color and counted using a Matlab (The MathWorks Inc., Natick, USA) script. The surface area covered by cells at 7.5 h and 5 days was calculated semi-automatically using Matlab. From each image a 0.490 mm^2 area containing 16 square patterns (0.097 mm^2 of patterns) was selected. The cells and patterned material squares ("objects") could be separated from the uncovered silicon background by identifying their edges with Canny edge detection operator. The areas inside the edges represent either cells or patterned material. Surface covered by objects smaller than 250 pixels (less than 230 μm^2, too small to represent cells) was considered uncovered. Edges were marked on the image that contained object pixels (a cell or a pattern) and uncovered silicon background. This image was compared to the original image and uncovered square pattern surface was manually separated from cell–covered surface. Some images needed extra manual segmentation. The accuracy of the method is not 100%, but the

eventual errors are systematic, meaning that different samples can be compared against each other.

2.7 Staining of focal adhesions

All steps in staining described below 2.7–2.10 were conducted at room temperature unless otherwise mentioned. One of the patterned Ti, Ta, Cr, and AD samples cultured for 7.5 h and 5 days were used for staining of focal adhesions. After two washes in PBS the samples were fixed in 4% paraformaldehyde (PFA) in PBS for 10 min. Samples were washed twice in PBS, permeabilized for 10 min in 0.1% Triton X-100 in PBS and then washed twice in the same solution. Non-specific binding sites were blocked using normal goat serum diluted 1:10 in 0.1% bovine serum albumin (BSA) in PBS for 1 h. After normal goat serum was blotted away, samples were incubated in monoclonal mouse anti-human vinculin IgG [24] for 1 h and washed 3× in Triton X-100 in PBS. From this point forward all steps were performed in the dark. Samples were incubated for 30 min in Alexa-Fluor 488 conjugated goat anti–mouse IgG (Molecular Probes, Eugene, USA; 1:400 in BSA–PBS) and Phalloidin-586 (Invitrogen, Carlsbad, USA; 1:30 in BSA–PBS), washed 3× in PBS and counterstained with DAPI (1:1000 in dH_2O; Sigma) nuclear stain for 10 min. Samples were washed twice in PBS and once in dH_2O before mounting.

2.8 Alkaline phosphatase (ALP) staining

Fourteen day samples were washed twice in PBS and incubated for 1 h in Naphthol-AS-MX phosphate sodium salt (Sigma, 1 mg/ml) substrate and Fast red TR (Sigma, 1 mg/ml) chromogen in 0.1 M Tris buffer (pH 8). Samples were washed twice in PBS, fixed in 4% PFA in PBS for 15 min, washed 3× in dH_2O, permeabilized in Triton X-100 in PBS for 10 min, washed 3× in PBS, counterstained in DAPI (1:1000 in dH_2O) for 10 min, washed twice in PBS and once in dH_2O before mounting.

2.9 OC staining

Seventeen day samples were washed 3× in PBS and fixed in 4% PFA in PBS for 20 min. Samples were washed twice in PBS, permeabilized in Triton X-100 in PBS for 10 min and washed 3× in PBS before blocking in normal donkey serum (1:10 in 0.1% BSA–PBS) for 1 h. Samples were incubated in rabbit anti-human osteocalcin IgG (AbD Serotec 7060-1515; 1:40 in BSA–PBS) overnight at +4°C. After this all steps were performed in the dark. Samples were washed 3× in PBS and incubated in Alexa-Fluor 488-conjugated donkey anti-rabbit IgG diluted 1:100 in 0.1% BSA–PBS for 60 min. Samples were washed 3× in PBS and labeled for F-actin using Phalloidin-586 diluted 1:30 in 0.1% BSA–PBS for 20 min. Samples were washed twice with PBS and once in dH_2O before mounting.

2.10 Staining of bone mineral

Twenty-one day samples were washed twice with PBS and fixed in 4% PFA in PBS for 15 min. Samples were transferred to a glass Petri dish (acetone and xylene used in washes are strong solvents), washed 3× in dH_2O and stained in 2% Alizarin Red S (Sigma) for 2 min, rinsed 20× in acetone, 20× in acetone–xylene (1:1) and cleared in xylene before mounting.

2.11 Microscopy and photographing

After staining samples were picked up from the Petri dishes (mineralization assay) or 12-well microculture plates (all other assays) and gently dried by tipping their edge to paper. They were fixed to objective slides using superglue and mounted in Vectashield (vinculin, ALP and OC staining; Vector Laboratories, Ltd., Peterborough, England) or Mountex (bone mineral staining; Histolab, Göteborg, Sweden) and coverslipped. Cells were observed using Leitz Diaplan microscope (mineralization assay, Wetzlar, Germany) or Olympus fluorescence microscope (all other assays, Olympus, Tokyo, Japan) and appropriate fluorochromes filters. Same exposure times were used so that the images could be compared. ALP activity was imaged using excitation wavelength of 510–550 nm and Olympus filter U-MWG2, nucleus using 330–285 nm and U-MWU2 and osteocalcin using 460–495 nm and U-MWIBA3.

2.12 Statistical analysis

Error estimate was based on the standard deviation of the mean and statistically significant differences were tested using ANOVA. The number of samples was 16 for Ta, Ti and Cr and 12 for AD. All results are expressed as mean ± standard deviation of the mean.

3 Results

Statistically significant difference of one material against two of the other materials is denoted with the number sign (#) and against only one of the other materials with the plus sign (+) with the figure legends specifying which material differences were significant.

3.1 Sample characterization

At the nanometer level the average surface roughness (R_a) and the peak-to-valley roughness (R_{pv}) values of AD were

statistically significantly lower compared to all other coatings ($P < 0.001$). Differences between Cr and Ta or Ti were statistically significant ($P < 0.001$) (Table 1). However, differences are very small and all the studied surfaces are very smooth, i.e. they have mirror finish. Contact angles and surface energy components of coatings and pure p-type silicon are shown in Table 1.

3.2 Early adhesion of hMSCs

Based on visual inspection (Fig. 1a–d) of early 7.5 h adhesion hMCS seemed to prefer the patterns to the background and they tended to be aligned along the edges of the patterns often assuming a squared shape. The guiding effect is clear on all materials and is analyzed in more detailed below.

3.2.1 Cell number density

Figure 2a presents the cell density on the patterns and on the silicon background at 7.5 h. On all materials, except for Ti, the density of the cells was 3.0–3.5 times higher than on the background ($P < 0.0003$ for all). Thus, the guiding effect of the patterns on adherence was clear for all other materials, but the density of the cells on the Ti patterns did not differ from the density of the cells on the silicon background ($P = 0.14$). The only difference between different materials was the marginal difference of the cell density on the Ti patterns compared to Cr and Ta patterns ($P < 0.06$). The average MSC density shown in the Fig. 2a seems to be low when compared to cells grown on the patterns. It is to be noted that the MSCs preferred the biomaterials tested over the silicon background, but that the area of the background formed ~80% of the sample areas whereas the squared patterns formed only ~20% of the sample area. However, also the average cell number densities were calculated and they demonstrate that there were no statistically significant differences in the average cell number densities (P-value range 0.32–0.93), which indicates that the seeding of the cells had been successful and uniform on all samples.

3.2.2 Surface area covered by the cells

The analysis of the surface area (of patterns and silicon background) covered by the cells at 7.5 h (Fig. 2b) gave results congruent with the analysis of the cell density described above. The guiding effect was also in this respect clear on all the materials ($P < 0.02$) except for Ti ($P = 0.46$). Furthermore, the coverage analysis disclosed significant differences between materials. The surface area of the Ti patterns covered by cells was smaller than that of the Cr and Ta patterns ($P < 0.03$ for both). The surface area of the silicon background covered by hMSCs was lower on samples containing Ti patterns than on samples containing AD patterns ($P < 0.02$).

3.2.3 Size of the cells

The mean diameter of the cell on the silicon background, assuming in these calculations a round shape, was 102 μm (corresponding to the surface area of approximately

Table 1 Surface roughness values (peak-to-valley roughness (R_{pv}) and average surface roughness (R_a)), contact angles and surface free energy components for the surfaces of different test materials

Materials	Roughness		Contact angle, θ (°)		Surface free energy components (mJ/m^2)		
	R_{pv} (nm)[a]	R_a (nm)[a]	θ^{water}	$\theta^{diiodomethane}$	γ_S^D	γ_S^P	γ_S
AD, smooth	2.4 ± 1.0	0.3 ± 0.1	67.4 ± 2.0	36.1 ± 1.0	41.5 ± 0.5	8.1 ± 0.8	49.6 ± 1.2
AD, patterned			63.6 ± 1.6[b]	45.5 ± 1.3[b]	36.7 ± 0.7[b]	11.6 ± 0.8[b]	48.3 ± 1.0
Ti, smooth	11.1 ± 1.5	1.8 ± 0.2	67.6 ± 2.0	35.4 ± 1.2	41.8 ± 0.5	7.9 ± 0.9	49.7 ± 1.1
Ti, patterned			65.1 ± 1.1	48.9 ± 1.2[b,c]	34.9 ± 0.7[b,c]	11.4 ± 0.8[b,e]	46.3 ± 0.3[b,c]
Ta, smooth	8.5 ± 2.0	1.5 ± 0.3	64.1 ± 1.6[c,d,e]	33.4 ± 1.4[c,e]	42.8 ± 0.6[c,e]	9.3 ± 0.6[e]	52.1 ± 1.1[c,d,e]
Ta, patterned			62.7 ± 1.5[e]	46.7 ± 1.2[b]	36.1 ± 0.6[b]	12.3 ± 0.8[b,e]	48.4 ± 0.9[b,d,e]
Cr, smooth	5.4 ± 1.0	0.8 ± 0.1	71.2 ± 1.1[c,d]	37.7 ± 1.5	40.8 ± 0.7	6.6 ± 0.5[c]	47.3 ± 0.7[c,d]
Cr, patterned			68.8 ± 1.8[c,d]	46.6 ± 1.3[b]	36.1 ± 0.7[b]	9.1 ± 1.0[b,c]	45.2 ± 0.7[b,c]
Silicon	1.4 ± 0.5	0.2 ± 0.1	32.4 ± 1.9	35.6 ± 1.1	41.8 ± 0.5	26.8 ± 0.4	68.5 ± 0.8

Values are the mean ± SD

[a] $P < 0.005$ between all materials

[b] $P < 0.05$ vs. smooth counterpart

[c] $P < 0.05$ vs. AD with the same surface topography (smooth or patterned)

[d] $P < 0.05$ vs. Ti with the same surface topography

[e] $P < 0.05$ vs. Cr with the same surface topography

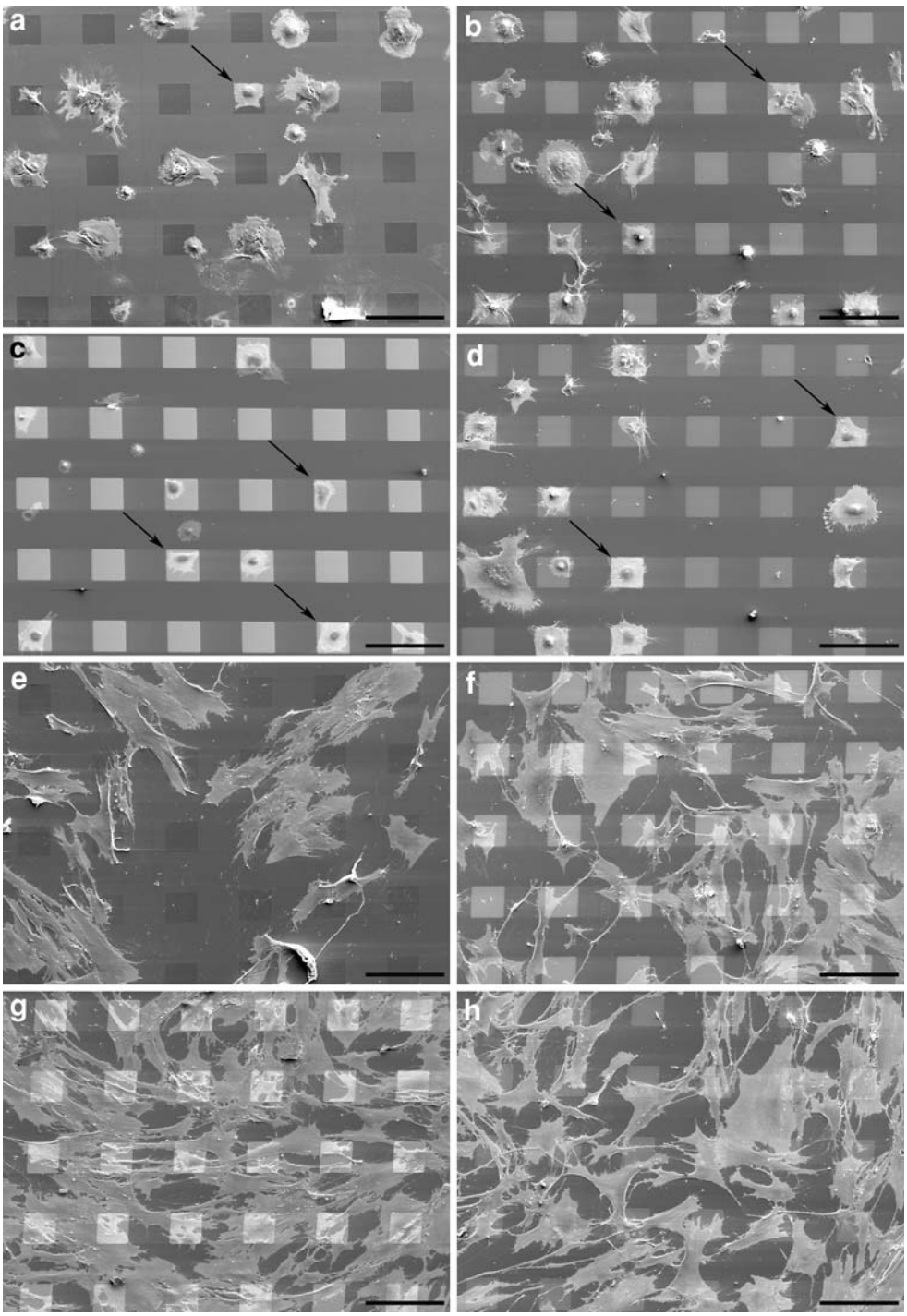

Fig. 1 Mesenchymal stem cells after 7.5 h incubation (**a–d**) and 5 days incubation (**e–h**) on patterned **a**, **e** amorphous diamond, **b**, **f** chromium, **c**, **g** tantalum and **d**, **h** titanium surfaces. Scale bar is 200 μm. Arrows point to some of the cells, which were aligned along the edges of the patterns and thus assumed squared shapes

8000 μm^2) being clearly larger than the 68 μm (surface area 3600 μm^2) of the cells on the patterns (Fig. 2c, $P < 0.02$ for all). There were no statistically significant differences between patterns produced of different materials (P-value range 0.55–0.96).

3.3 Spreading of hMSCs

To study spreading of the hMSCs they were incubated for 5 days (approximately 80% confluence). According to the visual inspection at this stage the individual cells had

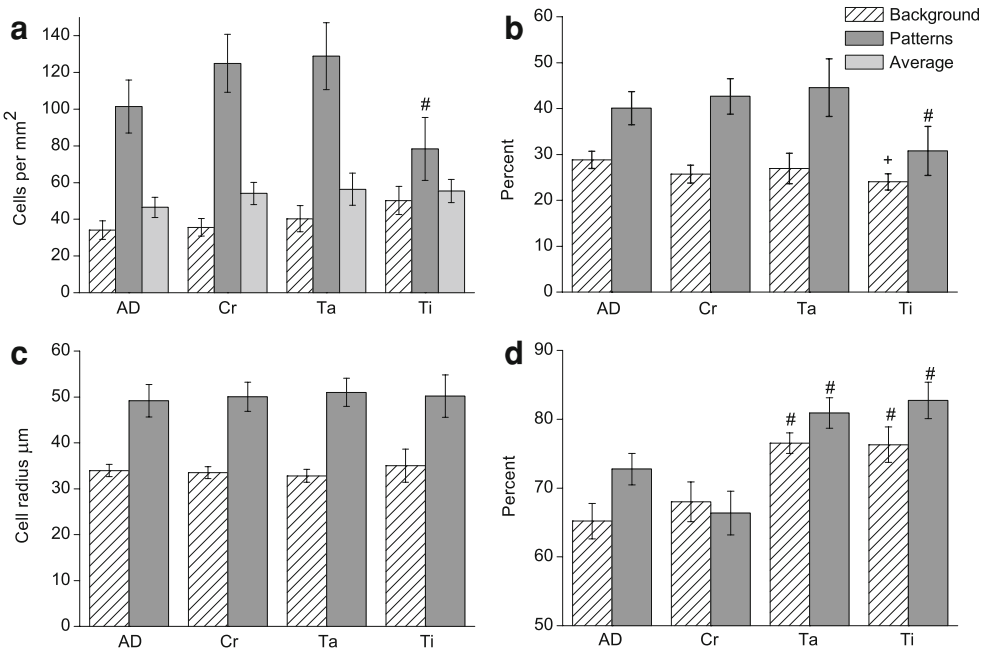

Fig. 2 **a** Density, **b** coverage and **c** size of hMSC at 7.5 h and **d** 5 days. A marginal (**a**) or a significant (**b**) difference compared to chromium and tantalum, and a significant difference compared to amorphous diamond and chromium (**d**) are denoted with # and a significant difference compared to amorphous diamond is denoted with + (**b**)

apparently already reached a size which greatly exceeds that of a singular square pattern (which is 5625 μm^2). Because of the large size of the cells and the difficulties in identification of the edges of the individual cells in subconfluent cell mats, it was not possible at 5 days to calculate the cell density or parameters reflecting the size of the individual cells on samples containing square patterns of different materials (Fig. 1e–h). Only the surface area of the square patterned materials covered by cells compared to the surface area of the silicon background covered by the cells was analyzed to see if perhaps still at this subconfluent stage some guiding effect could be discerned.

3.3.1 Surface area covered by the cells

At 5 days the guiding effect of the square patterned materials was not as clear as it was at 7.5 h. The surface area of the square patterns covered by the cells (Fig. 2d) was only 1–1.9 times higher than that of the silicon background and only the difference between the AD patterns and silicon background was significant ($P < 0.04$). The surface area covered by cells of the silicon background was higher on samples containing Ta and Ti patterns than on samples containing AD patterns ($P = 0.0005$ and $P = 0.006$) and on samples containing Cr patterns lower than on samples containing Ta and Ti patterns ($P = 0.014$ and $P = 0.04$). The ranking order of the surface area of the square patterns covered by cells was now Ti, Ta, AD and Cr. Differences between AD and Ti or Ta ($P < 0.02$), and between Cr and Ti or Ta ($P < 0.0008$) were significant.

3.4 Adhesion of hMSCs—focal adhesion staining

3.4.1 Early adhesion

At 7.5 h the actin filaments had already become well organized, but vinculin containing focal adhesions were still relatively few. Cells had already started to spread out attaching mostly to the corners of the square patterns as can be seen in Fig. 3a–d.

3.4.2 Spreading of the cells

At 5 days vinculin containing focal adhesions were already well developed (Fig. 3e–h). Actin cytoskeleton assumed an orange hue in overlay figures due to the green colored vinculin. Based on observation of our previous study with osteoblastic SaOS-2 cells [Kaivosoja et al., unpublished study] we expected to see preferential localization of vinculin containing focal adhesions on the square patterns, but hMSCs did not show such a preference for the patterns.

3.5 Osteogenic differentiation of hMSCs

Progression of osteogenic differentiation of hMSCs was confirmed by using well established lineage markers ALP, OC and bone mineral (Figs. 4, 5 and 6).

3.5.1 ALP activity

Red color represents the ALP activity and blue represents cell nuclei. At 14 days ALP was seen in all induced cells

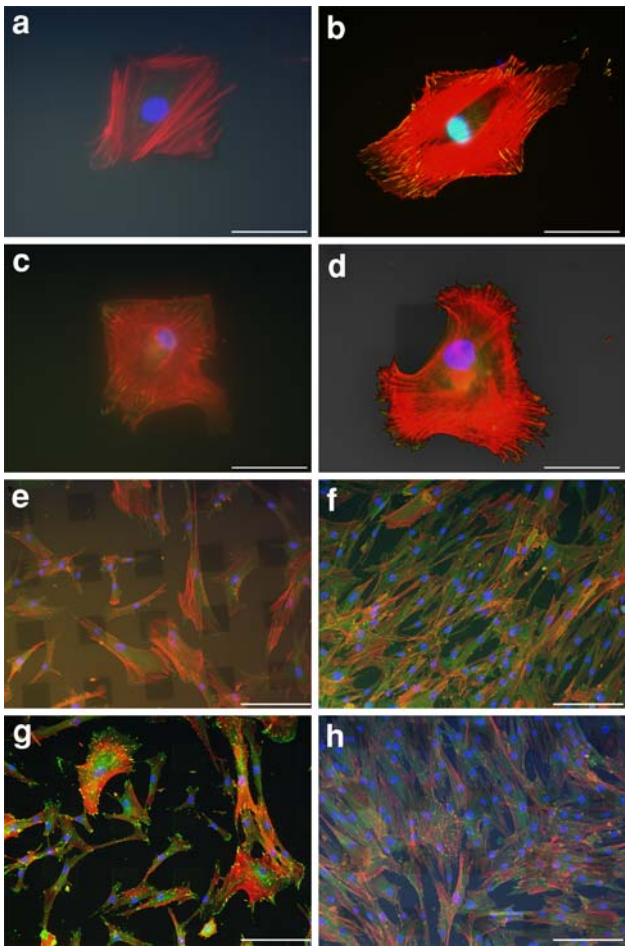

Fig. 3 Staining of mesenchymal stem cells at 7.5 h (**a–d**) and 5 days (**e–h**). Actin filaments of the cells stain red, cell nuclei blue and vinculin green. Samples: **a**, **e** amorphous diamond; **b**, **f** chromium; **c**, **g** tantalum; **d**, **h** titanium. Scale bar is 50 μm (**a–d**) or 200 μm (**e–h**)

(two middle rows), whereas the control hMSC cells did not stain (Fig. 4). There were no consistent differences between induced cells cultured on plain surface samples and induced cells cultured on the square patterns of patterned samples. When materials were compared with each other Ta containing samples seemed to have the greatest ALP activity.

3.5.2 Osteocalcin

Green color represent OC immunoreactivity and for clarity it is shown alone, without the strongly labeled actin cytoskeleton (which had red label as in Fig. 3). At 17 days OC was similarly seen in induced cells cultured on Cr, Ta and Ti, but not in induced cells cultured on AD, whereas the control hMSC cells did not stain (Fig. 5). There were no clear-cut differences between the patterned and plain samples.

3.5.3 Mineralization

Red color seen in the extracellular matrix represents bone mineral. At 21 days only induced samples contained extracellular bone mineral stain, whereas in the hMSC control cell samples only the cells were outlined without any extracellular bone mineral deposits (Fig. 6). Cultures on patterned samples contained much less bone mineral than cultures on plain surfaces. Bone mineral deposition was weak in cultures on plain AD surfaces, but Cr, Ta and Ti containing samples were similarly labeled.

4 Discussion

Surface roughness affects protein adsorption and cellular responses, for example osteoblastic cells prefer rough surfaces whereas fibroblasts favor smooth surfaces [25]. To produce two different types of coatings, metals and diamond ceramic, two different types of PVD methods were used: magnetron sputtering for metal coating and filtered pulsed plasma arc discharge for diamond-like carbon coating. However, roughness of the plain and patterned samples was in this work characterized in nanoscale, using AFM. This disclosed that all surfaces used in the present study were extremely smooth, with R_a values of less than 2 nm. Fibroblast [26] and hMSC [27] filopodia have a sensory role but the smallest features they sense are 10 nm-high islands. It thus seems that with R_a value differences <2 nm the only relevant topographical cues of the samples studied are the steps between the patterns and the background (≈ 20 nm). This refutes the risk that the clear-cut differences seen between different materials and patterns would have been due to differences in surface topography and instead suggests that the differences observed and discussed below are mediated by different chemical compositions and physical patterns of the materials studied. Interestingly, it has been described that pattern edges influence cell division, cell cytoskeleton and migration [28–32] and may play a role in hMSC differentiation, with the geometry of the patterns influencing adipogenesis of hMSCs [16] and its timing [33], quite in line with the current osteogenesis studies.

Materials and patterns had jointly a remarkable early guiding effect on hMSCs, which was reflected as early differences between the cell numbers on patterns and the intervening silicon background, mediated by preferential cellular adhesion to the metallic and AD patterns (and avoidance of the background silicon). This guiding effect was further reflected by the different sizes of the cells derived from the same seeder cells upon their attachment on different substrates, with small cells predominating on the biomaterial patterns, whereas cells were larger on the

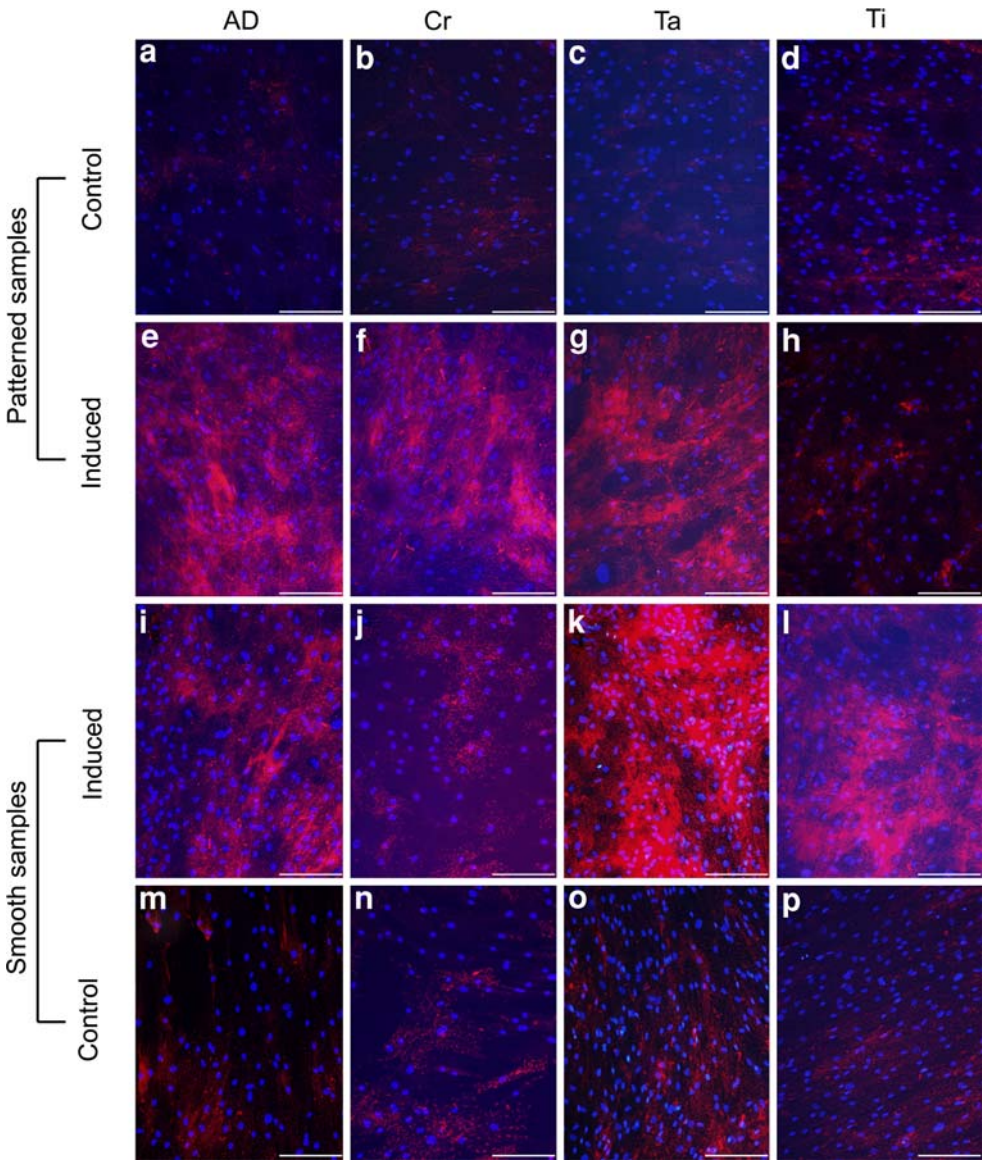

Fig. 4 Alkaline phosphatase staining of mesenchymal stem cells. Samples: **a–d** control cells and **e–h** induced cells on a patterned sample; **i–l** induced cells and **m–p** control cells on a plain sample. First column shows amorphous diamond, second column chromium, third column tantalum and fourth column titanium. Scale bar is 200 μm

silicon background. Microtubules keep growing along non-adhesive edges up to the next adhesive site but stop growing when they come into contact with an adhesive edge. This suggests that the shape of individual nonmigrating cells responds to the geometry and anisotropy of the external cell adhesive environment [29]. This phenomenon, physical constraints, might explain the differences in cell sizes on the relatively small square patterns and on the broader background. The adhesive nature of the process was confirmed by guided re-organization of the cellular actin cytoskeleton and focal adhesions so that cells on patterns preferred the very edges of these patterns. Guiding effect took therefore a clear-cut expression in the geometric, "engineered" square shape, which the generally rounded cells assumed on their material islands bordering to the silicon background. Similar observation has been made by Parker et al. [34], who used square islands of extracellular matrix in the presence of motility factors to study the effect of mechanical interactions between cells and their extracellular matrix (cell–substrate interactions) on cell migration. They observed that the cells preferentially extended lamellipodia, filopodia, and microspikes from their corners. These earlier reports and the current work indicate that these guiding effects are mediated by a direct physical cell–substrate contact. The number, size, surface area covered, cytoskeletal re-organization, vinculin-containing focal adhesions and cell shape all together indicate that, apart from the chemical composition of the substrate, also its physical shape and edges exert an effect on the hMSCs inhabiting them. These observations could be exploited to guide the migration of the cells, e.g. triangles could be used to guide the cells to migrate in a predefined direction.

When the current experiments were planned, it was thought that the square patterned material-on-silicon

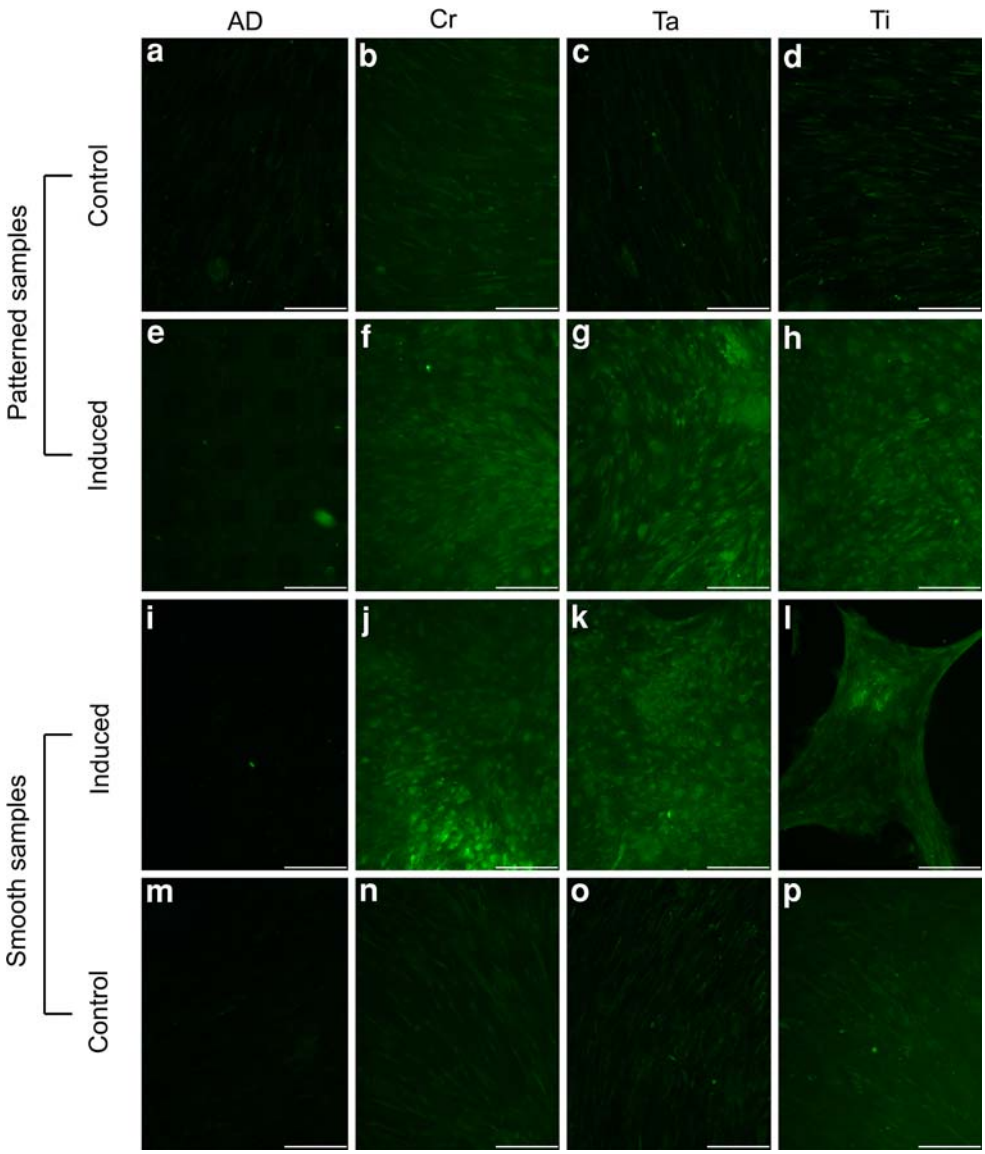

Fig. 5 Osteocalcin staining of mesenchymal stem cells. Samples: **a–d** control cells and **e–h** induced cells on a patterned sample; **i–l** induced cells and **m–p** control cells on a plain sample. First column shows amorphous diamond, second column chromium, third column tantalum and fourth column titanium. Scale bar is 200 μm

samples could also be used to standardize inter-experiment differences, which are often seen in cell culture experiments. It is a well known phenomenon that some variation can occur from one cell culture experiment to another although basically all steps are done following the same protocol. In other words, if the cells for some reason in one experiment grow more slowly than in another experiment, one could in principle correct this difference by calculating the patterns-to-silicon background ratio for the cell density. This approach has recently been successfully applied in bacterial culture experiments [35]. It was therefore somewhat of a surprise that the cell density on the very same silicon background varied statistically significantly depending on what type of material islands had been microfabricated to the sample. At 7.5 h the surface area of the background silicon covered by hMSCs was significantly lower on samples containing Ti than AD patterns, but by the 5th culture day this had been reversed. This suggests that apart from direct material-cell interactions, cells on material islands have remote interactions with cells growing on silicon background. Probably these interactions are mediated by some soluble growth regulating molecules released into the cell culture medium by the hMSC attached on the square patterns. Naturally cells growing on the silicon background can also influence cells growing on the patterned material islands, but because all samples tested shared this very same silicon background, differences between different patterned samples cannot be explained by such "reverse" cellular interactions.

Apart from capability of hMSCs to undergo asymmetrical cell divisions to be able to maintain their stemness, they also have a remarkable capability to differentiate along various lineages, e.g. to osteoblasts (pluripotency). Such osteogenic differentiation experiments are relatively

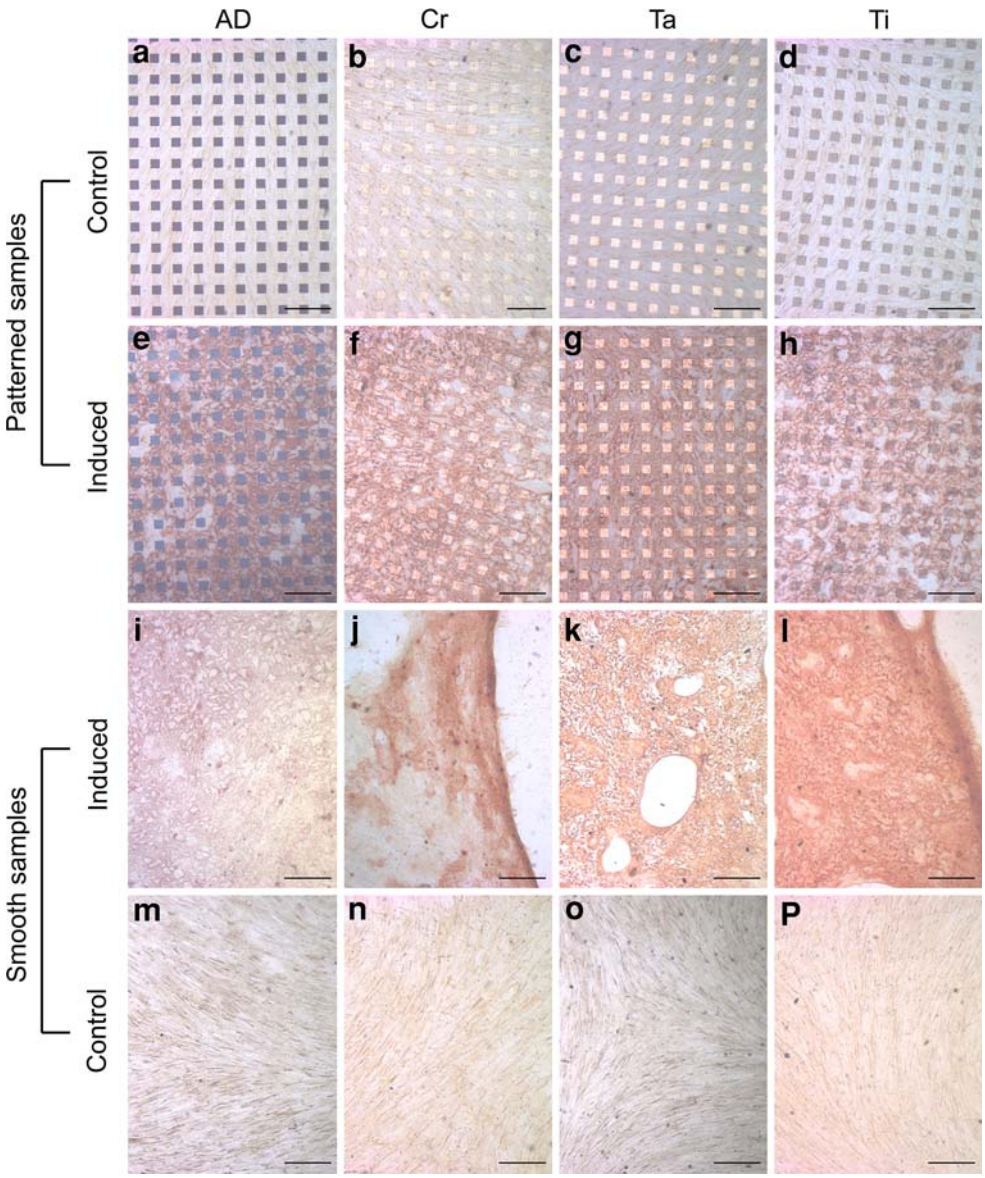

Fig. 6 Mineral staining of mesenchymal stem cell cultures. Mineralization of the cells stains red. Samples: **a**–**d** control cells and **e**–**h** induced cells on a patterned sample; **i**–**l** induced cells and **m**–**p** control cells on a plain sample. First column shows amorphous diamond, second column chromium, third column tantalum and fourth column titanium. Scale bar is 400 μm

time consuming, but provide information on long-term (weeks) cell–biomaterial/pattern interactions in contrast to the short-term (hours) and intermediate (days) effects seen in adhesion and spreading experiments discussed above. The passage number used in the present experiment seems high, but is not critical for osteogenic differentiation experiments because Wagner et al. [36] have shown that the propensity for osteogenic differentiation increased from the 7th to the 12th passage. Osteogenic differentiation was induced and followed by demonstration of well characterized osteogenetic markers of various differentiation stages developing sequentially, starting from the expression of ALP, followed by synthesis of OC and finally by deposition of bone mineral. In the checkerboard experiments AD, Ta, Ti and Cr were analyzed at 14, 17 and 21 days for these markers, respectively, as patterned and plain material surfaces. Ontogenesis was induced on patterned Ta, Ti and Cr samples, but not as effectively as on plain surfaces. The reason for this difference it not quite clear, but it seems reasonable to speculate that on plain surfaces the cells have the space they need to organize themselves to multicellular bone tissue-type structures, for which process the biocompatible Ta, Ti and Cr islands were not quite as good platforms. The pattern edge phenomenon may play a role here and can influence differentiation rate [16]. Also based on the work on microcontact printed fibronectin islands on polydimethylsiloxane it seems that the differentiation of hMSCs is controlled by the size of the islands. Adipogenesis took place only on small islands (1024 μm^2), whereas osteogenesis occurred only on large islands (10000 μm^2), with mixed results on intermediate-sized (2025 μm^2) islands [11]. We used intermediate pattern size

(5625 μm^2) and can also conclude that the pattern size may play a role for hMSC guidance and differentiation. Progenitor cells rely on spatial information for differentiation [17] and the balance between focal adhesion formation and other cell signaling phenomena may be critical in osteogenesis [18].

In spite of relatively competitive initial cell–AD interactions and development of ALP activity, the later stages of osteogenesis failed in samples containing patterned but also plain AD. Therefore, it seems that smooth and inert AD coating could be used for implants, which come into contact with bone but which need to be removed later, e.g. various fracture fixation devices, such as plates and screws. In this setting overgrowth of the implant by bone would complicate the implant removal. Contact angle measurements were performed to characterize the coatings in terms of their surface energy and their polar and dispersive components. Increased wettability with high surface free energies has been demonstrated to be beneficial regarding to short-term adhesion [37], spatial growth and mineralization [38] as well as differentiation of bone cells [39]. In this case, however, differences in surface energy cannot explain differences observed in hMSC responses.

In conclusion, the chemical composition and patterning of materials, which can also interact, can be used to regulate hMSC behaviour.

Acknowledgements The work was supported by Finska Läkaresällskapet, the National Graduate School of Musculoskeletal Diseases and Biomaterials, NMT ERA Net project "A new generation of titanium biomaterials", MATERA "Bioactive nanocomposite constructs for regeneration of articular cartilage", ESF "Regenerative Medicine", TEKES "Nanorobotics for medical diagnostics and therapy", EVO grants and Sigrid Jusélius Foundation. The authors acknowledge the staff of the Microsensor Laboratory of Applied Sciences for assistance with the microfabrication processes and AFM imaging. We thank Electron Microscopy Unit of the Institute of Biotechnology-University of Helsinki for providing laboratory facilities and VTT Technical Research Centre of Finland for sterilizing samples.

References

1. Curtis A, Wilkinson C. Topographical control of cells. Biomaterials. 1997;18:1573–83. doi:10.1016/S0142-9612(97)00144-0.
2. Flemming RG, Murphy CJ, Abrams GA, Goodman SL, Nealey PF. Effects of synthetic micro- and nano-structured surfaces on cell behavior. Biomaterials. 1999;20:573–88. doi:10.1016/S0142-9612(98)00209-9.
3. Mwenifumbo S, Li M, Chen J, Beye A, Soboyejo W. Cell/surface interactions on laser micro-textured titanium-coated silicon surfaces. J Mater Sci: Mater Med. 2007;18:9–23. doi:10.1007/s10856-006-0658-9.
4. Falconnet D, Csucs G, Michelle Grandin H, Textor M. Surface engineering approaches to micropattern surfaces for cell-based assays. Biomaterials. 2006;27:3044–63. doi:10.1016/j.biomaterials.2005.12.024.
5. Ito Y. Surface micropatterning to regulate cell functions. Biomaterials. 1999;20:2333–42. doi:10.1016/S0142-9612(99)00162-3.
6. Pittenger MF, Mackay AM, Beck SC, Jaiswal RK, Douglas R, Mosca JD, et al. Multilineage potential of adult human mesenchymal stem cells. Science. 1999;284:143–7. doi:10.1126/science.284.5411.143.
7. Lappalainen R, Santavirta SS. Potential of coatings in total hip replacement. Clin Orthop Relat Res. 2005;430:72–9. doi:10.1097/01.blo.0000150000.75660.ff.
8. Lappalainen R, Selenius M. Joint bearing surfaces and replacement joint design. In: Revell PA, editor. Joint replacement technology. Cambridge, UK: Woodhead Publishing Limited; 2008. p. 176–89.
9. Stiehler M, Lind M, Mygind T, Baatrup A, Dolatshahi-Pirouz A, Li H, et al. Morphology, proliferation, and osteogenic differentiation of mesenchymal stem cells cultured on titanium, tantalum, and chromium surfaces. J Biomed Mater Res A. 2008;86:448–58. doi:10.1002/jbm.a.31602.
10. Pirone DM, Qi L, Colecraft H, Chen CS. Spatial patterning of gene expression using surface-immobilized recombinant adenovirus. Biomed Microdevices. 2008;10:561–6. doi:10.1007/s10544-008-9166-7.
11. McBeath R, Pirone DM, Nelson CM, Bhadriraju K, Chen CS. Cell shape, cytoskeletal tension, and RhoA regulate stem cell lineage commitment. Dev Cell. 2004;6:483–95. doi:10.1016/S1534-5807(04)00075-9.
12. Hart A, Gadegaard N, Wilkinson CDW, Oreffo RO, Dalby MJ. Osteoprogenitor response to low-adhesion nanotopographies originally fabricated by electron beam lithography. J Mater Sci: Mater Med. 2007;18:1211–8. doi:10.1007/s10856-007-0157-7.
13. Berry CC, Curtis ASG, Oreffo ROC, Agheli H, Sutherland DS. Human fibroblast and human bone marrow cell response to lithographically nanopatterned adhesive domains on protein rejecting substrates. IEEE Trans Nanobiosci. 2007;6:201–9. doi:10.1109/TNB.2007.903457.
14. Kim SJ, Lee JK, Kim JW, Jung JW, Seo K, Park SB, et al. Surface modification of polydimethylsiloxane (PDMS) induced proliferation and neural-like cells differentiation of umbilical cord blood-derived mesenchymal stem cells. J Mater Sci: Mater Med. 2008;19:2953–62. doi:10.1007/s10856-008-3413-6.
15. Ber S, Köse ST, Hasirci V. Bone tissue engineering on patterned collagen films: an in vitro study. Biomaterials. 2005;26:1977–86. doi:10.1016/j.biomaterials.2004.07.007.
16. Luo W, Jones SR, Yousaf MN. Geometric control of stem cell differentiation rate on surfaces. Langmuir. 2008;24:12129–33. doi:10.1021/la802836g.
17. Dalby MJ, McCloy D, Robertson M, Wilkinson CD, Oreffo RO. Osteoprogenitor response to defined topographies with nanoscale depths. Biomaterials. 2006;27:1306–15. doi:10.1016/j.biomaterials.2005.08.028.
18. Sjöström T, Dalby MJ, Hart A, Tare R, Oreffo RO, Su B. Fabrication of pillar-like titania nanostructures on titanium and their interactions with human skeletal stem cells. Acta Biomater. 2009;5:1433–41. doi:10.1016/j.actbio.2009.01.007.
19. Anttila A, Salo J, Lappalainen R. High adhesion of diamond-like films achieved by the pulsed arc-discharge method. Mater Lett. 1995;24:153–6. doi:10.1016/0167-577X(95)00071-2.
20. Anttila A, Lappalainen R, Tiainen V, Hakovirta M. Superior attachment of high-quality hydrogen-free amorphous diamond films to solid materials. Adv Mater. 1997;9:1161–4. doi:10.1002/adma.19970091507.
21. Owens DK, Wendt RC. Estimation of the surface free energy of polymers. J Appl Polym Sci. 1969;13:1741–7. doi:10.1002/app.1969.070130815.
22. Oliveira AL, Malafaya PB, Reis RL. Sodium silicate gel as a precursor for the in vitro nucleation and growth of a bone-like

apatite coating in compact and porous polymeric structures. Biomaterials. 2003;24:2575–84. doi:10.1016/S0142-9612(03)00060-7.
23. Malaval L, Liu F, Roche P, Aubin JE. Kinetics of osteoprogenitor proliferation and osteoblast differentiation in vitro. J Cell Biochem. 1999;74:616–27. doi:10.1002/(SICI)1097-4644(19990915)74:4<616::AID-JCB11>3.0.CO;2-Q.
24. Lehto V-P, Virtanen I. Vinculin in cultured bovine lens-forming cells. Cell Differ 1985;16:153–60.
25. Kunzler TP, Huwiler C, Drobek T, Vörös J, Spencer ND. Systematic study of osteoblast response to nanotopography by means of nanoparticle-density gradients. Biomaterials. 2007;28:5000–6. doi:10.1016/j.biomaterials.2007.08.009.
26. Dalby MJ, Riehle MO, Johnstone H, Affrossman S, Curtis AS. Investigating the limits of filopodial sensing: a brief report using SEM to image the interaction between 10 nm high nano-topography and fibroblast filopodia. Cell Biol Int. 2004;28:229–36. doi:10.1016/j.cellbi.2003.12.004.
27. Dalby MJ, McCloy D, Robertson M, Agheli H, Sutherland D, Affrossman S, et al. Osteoprogenitor response to semi-ordered and random nanotopographies. Biomaterials. 2006;27:2980–7. doi:10.1016/j.biomaterials.2006.01.010.
28. Théry M, Racine V, Piel M, Pépin A, Dimitrov A, Chen Y, et al. Anisotropy of cell adhesive microenvironment governs cell internal organization and orientation of polarity. Proc Natl Acad Sci USA. 2006;103:19771–6. doi:10.1073/pnas.0609267103.
29. Jiang X, Bruzewicz DA, Wong A, Piel M, Whitesides GM. Directing cell migration with asymmetric micropatterns, Proc Natl Acad Sci USA. 2005;102:975–8. doi:10.1073/pnas.0408954102.
30. Hoover DK, Chan EWL, Yousaf MN. Asymmetric peptide nanoarray surfaces for studies of single cell polarization. J Am Chem Soc. 2008;130:3280–1. doi:10.1021/ja711016m.
31. Chan EWL, Yousaf MN. A photo-electroactive surface strategy for immobilizing ligands in patterns and gradients for studies of cell polarization. Mol Biosyst. 2008;4:746–53. doi:10.1039/b801394b.
32. Brock A, Chang E, Ho CC, LeDuc P, Jiang X, Whitesides GM, et al. Geometric determinants of directional cell motility revealed using microcontact printing. Langmuir. 2003;19:1611–7. doi:10.1021/la026394k.
33. Chaubey A, Ross KJ, Leadbetter RM, Burg KJ. Surface patterning: Tool to modulate stem cell differentiation in an adipose system. J Biomed Mater Res B Appl Biomater. 2008;84:70–8. doi:10.1002/jbm.b.30846.
34. Parker KK, Brock AL, Brangwynne C, Mannix RJ, Wang N, Ostuni E, et al. Directional control of lamellipodia extension by constraining cell shape and orienting cell tractional forces. FASEB J. 2002;16:1195–2004. doi:10.1096/fj.02-0038com.
35. Levon J, Myllymaa K, Kouri V-P, Rautemaa R, Kinnari T, Myllymaa S, et al. Patterned macroarray plates in comparison of bacterial adhesion inhibition of tantalum, titanium, and chromium compared with diamond-like carbon, J Biomed Mater Res Part A. doi:10.1002/jbm.a.32486.
36. Wagner W, Horn P, Castoldi M, Diehlmann A, Bork S, Saffrich R, et al. Replicative senescence of mesenchymal stem cells: a continuous and organized process. PLoS ONE. 2007;3:e2213. doi:10.1371/journal.pone.0002213.
37. Khang D, Lu J, Yao C, Haberstroh KM, Webster TJ. The role of nanometer and sub-micron surface features on vascular and bone cell adhesion on titanium. Biomaterials. 2008;29:970–83. doi:10.1016/j.biomaterials.2007.11.009.
38. Lim JY, Shaughnessy MC, Zhou Z, Noh H, Vogler EA, Donahue HJ. Surface energy effects on osteoblast spatial growth and mineralization. Biomaterials. 2008;29:1776–84. doi:10.1016/j.biomaterials.2007.12.026.
39. Eriksson C, Nygren H, Ohlson K. Implantation of hydrophilic and hydrophobic titanium discs in rat tibia: cellular reactions on the surfaces during the first 3 weeks in bone. Biomaterials. 2004;25:4759–66. doi:10.1016/j.biomaterials.2003.12.006.